A soluble activin type IIA receptor induces bone formation and improves skeletal integrity

R. Scott Pearsall*†, Ernesto Canalis‡, Milton Cornwall-Brady*, Kathryn W. Underwood*, Brendan Haigis*, Jeffrey Ucran*, Ravindra Kumar*, Eileen Pobre*, Asya Grinberg*, Eric D. Werner*, Vaida Glatt§, Lisa Stadmeyer‡, Deanna Smith‡, Jasbir Seehra*, and Mary L. Bouxsein§

*Acceleron Pharma, Inc., 149 Sidney Street, Cambridge, MA 02139; ‡Department of Research, St. Francis Hospital and Medical Center, 114 Woodland Street, Hartford, CT 06105; and §Orthopedic Biomechanics Laboratory, Beth Israel Deaconess Medical Center and Harvard Medical School, Boston, MA 02215

Edited by John T. Potts, Jr., Massachusetts General Hospital, Charlestown, MA, and approved March 21, 2008 (received for review November 29, 2007)

Diseases that affect the regulation of bone turnover can lead to skeletal fragility and increased fracture risk. Members of the TGF-β superfamily have been shown to be involved in the regulation of bone mass. Activin A, a TGF-β signaling ligand, is present at high levels in bone and may play a role in the regulation of bone metabolism. Here we demonstrate that pharmacological blockade of ligand signaling through the high affinity receptor for activin, type II activin receptor (ActRIIA), by administration of the soluble extracellular domain of ActRIIA fused to a murine IgG2a-Fc, increases bone formation, bone mass, and bone strength in normal mice and in ovariectomized mice with established bone loss. These observations support the development of this pharmacological strategy for the treatment of diseases with skeletal fragility.

anabolic | osteoporosis | TGF-β | therapeutic

Bone remodeling is mediated by the concerted activities of bone-resorptive cells (osteoclasts) and bone-forming cells (osteoblasts) (1). Skeletal fragility in osteoporosis or cancer-induced bone loss caused by an imbalance in bone remodeling is a significant cause of morbidity and mortality worldwide. Currently, two classes of therapeutic agents are used to treat skeletal fragility: (*i*) antiresorptives, such as calcitonin, estrogen, selective estrogen receptor modulators, and bisphosphonates; and (*ii*) the anabolic agent teriparatide (parathyroid hormone; PTH 1–34). Antiresorptive therapies act by diminishing osteoclast activity, thereby decreasing the rate of bone resorption (2). Although antiresorptive therapies are effective at reducing bone loss and decreasing fracture risk, these agents fail to promote the replacement of lost bone (3, 4). Additionally, because osteoclasts participate in repair of microdamage that is generated with daily activity, there is concern that prolonged suppression of bone resorption by bisphosphonates and other antiresorptive agents may disrupt this normal process and lead to an increased accumulation of microdamage, eventually weakening the bone (5, 6).

In comparison, anabolic agents improve bone mass and strength by stimulating osteoblast-mediated bone formation and thus represent an attractive alternative to antiresorptive therapies. At present, only a single anabolic agent, teriparatide (PTH 1–34), is available to treat osteoporosis (7, 8). Despite its proven efficacy for improving bone mass and reducing fracture risk (9), the clinical use of teriparatide has been limited because of the burden of daily injections (9, 10).

We and others have evaluated the role of activin and activin antagonists in bone metabolism. The activin proteins are members of the transforming growth factor-β/bone morphogenetic protein (TGF-β/BMP) superfamily of signaling molecules, which have long been associated with bone metabolism. BMP-2 and BMP-7 are members of this family with clinically proven bone-forming activity as locally acting bone anabolic agents when surgically implanted as a device in a collagen-based matrix (11–13).

Activin was originally described as a factor that promoted the release of FSH from the pituitary (14). Activin is a homodimeric molecule that signals by binding with high affinity to a type II activin receptor (ActRIIA) followed by the recruitment of a type I receptor (ALK4) (15, 16). Activated ALK4 triggers the phosphorylation of Smad 2/3, which associates with Smad 4, forming a complex that translocates to the nucleus to regulate gene expression.

Inhibin is a related molecule produced in the ovary, originally described as a factor that inhibited the release of FSH by the pituitary (17). Inhibin is a heterodimeric molecule comprised of an activin β-subunit disulfide-linked to an inhibin α-subunit. Inhibin binds to the coreceptor β-glycan, then subsequently to ActRIIA, preventing activin from binding (18, 19). Inhibin thus serves as a competitive antagonist of ActRIIA (20, 21).

Activin A is one of the most abundant TGF-β/BMP family member proteins found in bone (22) and functions as a paracrine hormone, whereas inhibin is found at its highest levels in the gonads and acts primarily as an endocrine factor. The role of these two proteins in bone metabolism is not well understood. There is abundant evidence that activin can stimulate the formation of osteoclasts in bone marrow-derived cultures and that the inhibition of activin in these cultures by inhibin or soluble receptor antagonists restores osteoclastogenesis (23, 24). The effect of activin on osteoblasts is less clear, with several conflicting reports in the literature. There are some studies demonstrating a positive effect of activin on osteoblastogenesis (21), but recent studies provide evidence that activin inhibits osteoblast-mediated mineralization. This inhibition is reversed by the addition of the activin antagonist follistatin (25).

Activin also has been reported to stimulate bone formation directly in wild-type animals. Direct administration of activin into fracture sites increased callus formation, leading to increased healing and bone strength, suggesting a direct stimulatory effect on bone formation (26). Systemic administration of activin to aged ovariectomized rats has been reported to increase vertebral bone mineral density (BMD) and strength to a similar extent as PTH (27). Data in support of activin as a potential negative regulator of bone mass come from studies exploring the role of inhibin in bone metabolism (28). Transgenic overexpression of inhibin, which blocks the interaction of activin and related

Author contributions: R.S.P., R.K., A.G., E.D.W., and M.L.B. designed research; R.S.P., E.C., M.C.-B., E.P., A.G., E.D.W., V.G., L.S., D.S., and M.L.B. performed research; K.W.U., B.H., and J.U. contributed new reagents/analytic tools; R.S.P., E.C., M.C.-B., R.K., E.P., A.G., E.D.W., V.G., L.S., D.S., and M.L.B. analyzed data; and R.S.P. and J.S. wrote the paper.

Conflict of interest statement: R.S.P., M.C.-B., K.W.U., B.H., J.U., R.K., E.P., A.G., E.D.W., and J.S. are full-time employees of Acceleron Pharma.

This article is a PNAS Direct Submission.

Freely available online through the PNAS open access option.

†To whom correspondence should be addressed. E-mail: spearsall@acceleronpharma.com.

This article contains supporting information online at www.pnas.org/cgi/content/full/0711263105/DCSupplemental.

ligands with the ActRIIA receptor, resulted in a dramatic increase in bone mass and strength mediated by an increase in bone formation (28).

Given the contrasting data, we have sought to better understand the role of activin and related ligands that signal through the ActRIIA receptor in bone metabolism by administering a soluble ActRIIA receptor antagonist to adult mice.

Results

Construction and Purification of an ActRIIA–mFc Fusion Protein. The ActRIIA–mFc fusion protein was purified from conditioned medium by sequential column chromatography as described below. SDS/PAGE analysis showed a single protein band with a molecular mass of ≈106 kDa, under nonreducing conditions and of ≈57 kDa under reducing conditions (data not shown).

The binding affinity of the purified ActRIIA–mFc to activin A was determined by using a Biacore 3000 biosensor. To collect detailed kinetic information, a concentration series of activin A was injected over immobilized ActRIIA–mFc and a reference surface. A simple 1:1 interaction model provided an excellent fit to the data, as shown by the overlay of the simulated binding responses [red lines, supporting information (SI) Fig. S1*A*]. The K_D of activin A binding to the ActRIIA–mFc was determined to be 3.39 e^{-12} M (Fig. S1*A*).

To evaluate the ability of the purified ActRIIA–mFc to antagonize activin-induced Smad signaling, a reporter gene assay was performed by using a human rhabdomyosarcoma cell line (A204) transfected with pGL3(CAGA)12-luc, a Smad 2/3-responsive construct (29), and pRL-CMV-luc as internal control. The cells were treated with activin A in the presence or absence of ActRIIA–mFc and assayed for luciferase activity after 6 h (Fig. S1*B*). ActRIIA–mFc inhibited activin A activity in a dose-dependent manner with an inhibitory concentration (IC_{50}) of 22 ng/ml (≈275 pM) by using 10 ng/ml (≈400 pM) activin A. These results are similar to those reported in previous studies of ActRIIA-binding affinities (25, 26). The data demonstrate that the purified ActRIIA–mFc fusion protein inhibited activin-induced signaling through the Smad pathway.

To test the function of ActRIIA–mFc in osteoclastogenesis, RAW246.7 cells were induced to differentiate by the addition of receptor activator of nuclear factor κb ligand (RANKL) and macrophage colony-stimulating factor (MCSF). The addition of activin (20 ng/ml) increased tartrate-resistant acid phosphatase (TRAP) expression, indicating an increase in osteoclast differentiation (Fig. S1*C*). The addition of 20 μg/ml ActRIIA–mFc inhibited activin-dependent osteoclast differentiation and restored TRAP expression to the levels of RANKL/MCSF differentiation.

We also assessed the ability of ActRIIA–mFc to inhibit activin function in osteoblasts by using normal human osteoblast (NHOst) cells. Cells were induced to differentiate by the addition of medium containing 100 nM dexamethasone and 10 nM β-glycerol phosphate. The addition of 50 ng/ml activin A to the differentiation medium at the beginning of the culture inhibited mineralized nodule formation, as reported previously (25). The addition of 20 μg/ml ActRIIA–mFc to the differentiation medium at the same time as activin A restored the ability of the osteoblasts to differentiate and form mineralized nodules (Fig. S1*D*).

***In Vivo* Effects of ActRIIA–mFc in Normal Mice.** To assess the skeletal response to *in vivo* activin inhibition, 12-week-old gonadally intact female C57BL/6N female mice received twice weekly i.p. injections of ActRIIA–mFc (10 mg/kg) or vehicle (VEH, PBS). Mice were euthanized after 2, 4, 6, and 12 weeks of treatment, and bones were assessed by static and dynamic histomorphometry, microcomputed tomography (μCT), and biomechanical testing. Static histomorphometry of trabecular bone in the distal femoral metaphysis showed that ActRIIA–mFc increased trabecular bone volume by 45%, 120%, 130%, and 248% versus VEH at 2, 4, 6, and 12 weeks, respectively (Fig. 1*A*; $P \leq 0.01$). The increase in trabecular bone volume was due to an increase in both trabecular number (TbN) and trabecular thickness (TbTh) (Fig. 1 *B* and *C*; $P \leq 0.01$ for both). The eroded surface per bone surface (ES/BS), osteoblast number per bone perimeter (Nob/Bpm), and osteoclast number per bone perimeter (Noc/Bpm) were decreased by ActRIIA–mFc treatment at two weeks ($P \leq 0.01$) but did not differ from VEH thereafter (Fig. 1 *D–F*). The increased trabecular bone volume was secondary to an increase in bone formation because ActRIIA–mFc-treated mice exhibited a significant increase in mineralizing surface per bone surface (MS/BS) (80–120%), mineral apposition rate (MAR) (14–25%), and bone-formation rate (BFR, 115–155%) relative to VEH-treated mice over the course of the study (Fig. 1 *G–I*; $P \leq 0.01$ for all). Representative images of von Kossa-stained femurs at 6 weeks of treatment are shown in Fig. 1*J*. Consistent with the histomorphometry, serum osteocalcin, a marker of bone formation, was increased after 2 and 4 weeks of ActRIIA–mFc treatment (Fig. 1*K*). In comparison, serum TRAP5b levels, which reflect osteoclast cell number, were unchanged after 2 weeks but began increasing after 4 weeks of ActRIIA–mFc treatment (Fig. 1*L*), indicating an increase of bone formation followed by an increase in osteoclastogenesis.

Confirming the histomorphometric results of increased trabecular bone volume, μCT of the fifth lumbar (L5) vertebrae revealed that mice treated with ActRIIA–mFc had greater trabecular bone volume when compared with VEH-treated mice (8%, 29%, 39%, and 51% after 2, 4, 6, and 12 weeks, respectively, Fig. 2*A*). The increase was mainly due to increased trabecular number (18%, 25%, and 48% at weeks 4, 6, and 12; $P \leq 0.01$), and trabecular thickness (Fig. 2 *B* and *C*; $P \leq 0.05$). Representative images from the μCT analysis are shown for VEH and ActRIIA–mFc after 6 weeks of treatment (Fig. 2*D*). To examine the impact of increased trabecular bone volume on bone strength, compression testing of the L5 vertebrae was performed. Mice treated with ActRIIA–mFc had greater compression strength (25–66%, Fig. 2*E*) and absorbed more energy (66–167%, Fig. 3*F*) when compared with VEH. Taken together, these data indicate that in normal adult mice, ActRIIA–mFc stimulates bone formation, resulting in increased trabecular bone mass and strength.

ActRIIA–mFc Administration to Ovariectomized Mice. To further explore the effects of activin inhibition in a disease-state model, we determined the skeletal effects of ActRIIA–mFc in estrogen-deficient mice with established bone loss. Four-week-old C57BL/6 mice underwent ovariectomy (OVX) or sham (SHAM) surgery. After an 8-week period for bone loss to occur, mice were treated twice per week for 12 weeks with ActRIIA–mFc (10 mg/kg, i.p.) or VEH. *In vivo* pQCT measurements at the proximal tibia before treatment showed that trabecular bone density was ≈20% lower in OVX mice when compared with SHAM mice, indicating that ovariectomy had induced osteopenia (Fig. 3*A*, $P \leq 0.01$). Four weeks after ActRIIA–mFc treatment, trabecular bone density (TbBMD) was increased in the proximal tibia in both OVX and SHAM mice relative to VEH (Fig. 3 *A* and *B*; $P \leq 0.01$). At the end of 12 weeks of treatment, TbBMD in ActRIIA–mFc-OVX mice had increased 12% versus baseline ($P \leq 0.01$), whereas TbBMD in OVX-VEH mice showed a 15% decrease ($P \leq 0.01$) from baseline, for a net difference in TbBMD of 27% in between VEH control and ActRIIA–mFc-treated mice. In SHAM mice, ActRIIA–mFc treatment increased TbBMD by 27% relative to baseline ($P \leq 0.01$), consistent with its anabolic activity. At the end of 12 weeks of treatment with ActRIIA–mFc, OVX mice had TbBMD levels

PHARMACOLOGY

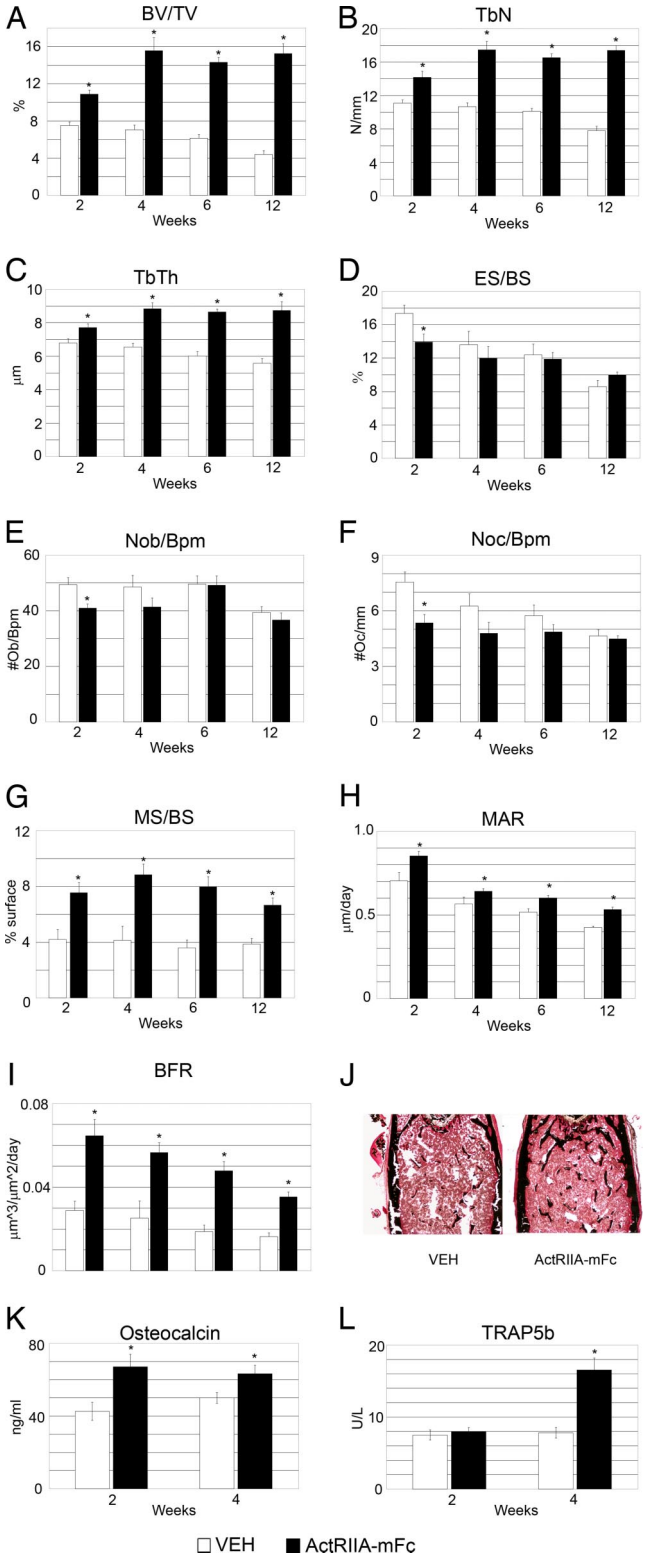

Fig. 1. ActRIIA–mFc treatment increases trabecular bone formation in normal mice. Static and dynamic histomorphometry parameters were measured in the distal femur. Open bars represent VEH-treated mice, and filled bars represent ActRIIA–mFc-treated mice. (*A*) Tb BV/TV (%). (*B*) Trabecular number (mm^{-1}). (*C*) Trabecular thickness (μm). (*D*) ES/BS (%). (*E*) Nob/Bpm (mm^{-1}). (*F*) Noc/Bpm (mm^{-1}). (*G*) MS/BS (%). (*H*) Mineral apposition rate (μm/day). (*I*) Bone formation rate ($\mu m^3/\mu m^2$/day). (*J*) Representative images from von Kossa staining of the femurs at 6 weeks. (*K* and *L*) Serum osteocalcin levels (ng/ml) (*K*) and TRAP5b levels (units/liter) (*L*) as measured by ELISA. All results are presented as the mean ± SEM. *, $P < 0.01$.

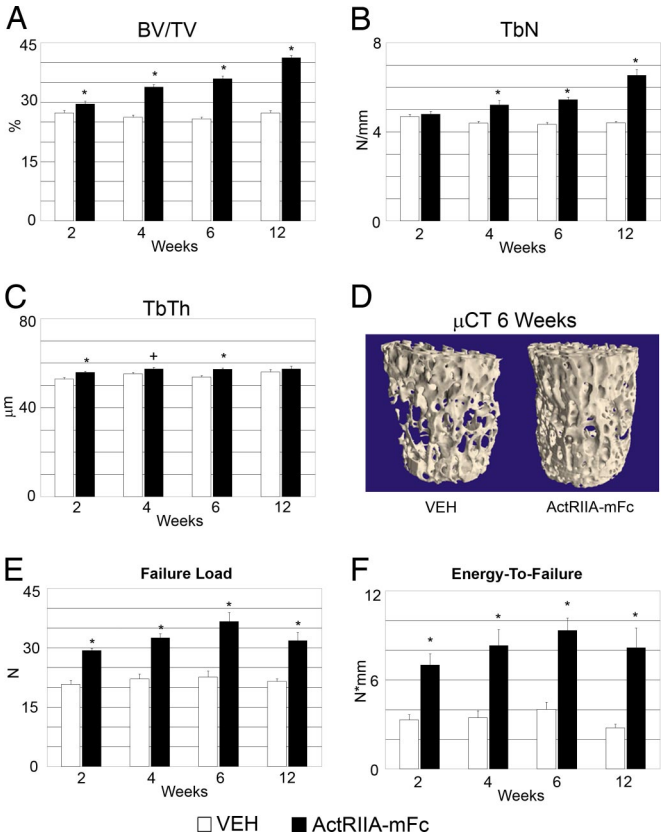

Fig. 2. *Ex vivo* μ and biomechanical analysis of the fifth lumbar vertebrae of ActRIIA–mFc-treated mice. Open bars represent VEH-treated mice, and filled bars represent ActRIIA–mFc-treated mice. (*A*) Tb BV/TV (%). (*B*) Trabecular number (mm^{-1}). (*C*) TbTh (μm). (*D*) Representative three-dimensional μCT images of vertebrae from mice treated for 6 weeks with VEH or ActRIIA–mFc. (*E*) Vertebral failure load (N) from compression testing. (*F*) Energy-to-failure (N × nmm) from compression testing. All results are presented as the mean ± SEM. *, $P < 0.01$; +, $P < 0.05$.

comparable with SHAM-VEH mice ($P = 0.1$), indicating a reversal of the osteopenic phenotype.

Similarly, μCT of the L5 vertebrae revealed that OVX-VEH mice had reduced trabecular bone volume (Tb BV/TV) 20% when compared with SHAM-VEH mice ($P \leq 0.01$), indicating that OVX had successfully induced osteopenia (Fig. 3*C*). Both OVX (+58%) and SHAM (+51%) ActRIIA–mFc-treated mice had significantly higher vertebral Tb BV/TV than their respective VEH-treated controls (Fig. 3*C*, $P \leq 0.01$ for both). Furthermore, trabecular bone volume was higher in OVX mice treated with ActRIIA–mFc than in age-matched VEH-SHAM controls ($P \leq 0.01$). Representative μCT images of the vertebrae from each treatment group are shown in Fig. 3*D*. A similar effect on trabecular bone was seen in the distal femur, where Tb BV/TV was significantly increased in ActRIIA–mFc-treated mice when compared with VEH controls (295% in OVX, 180% in SHAM, $P \leq 0.01$ for both). Compression testing of the L5 vertebrae confirmed that ActRIIA–mFc treatment improved both the strength and the energy-absorbed-to-failure in OVX and SHAM mice (Fig. 3 *E* and *F*, $P \leq 0.01$). Vertebral compressive strength of OVX mice treated with ActRIIA–mFc did not differ from age-matched SHAM-VEH controls ($P = 0.1$), whereas the OVX-VEH mice were significantly weaker than SHAM-VEH ($P \leq 0.01$).

To identify effects of ActRIIA–mFc treatment on cortical bone, μCT analysis of the mid-femoral diaphysis was performed (Fig. 4*A*). Cortical thickness was significantly reduced in OVX-

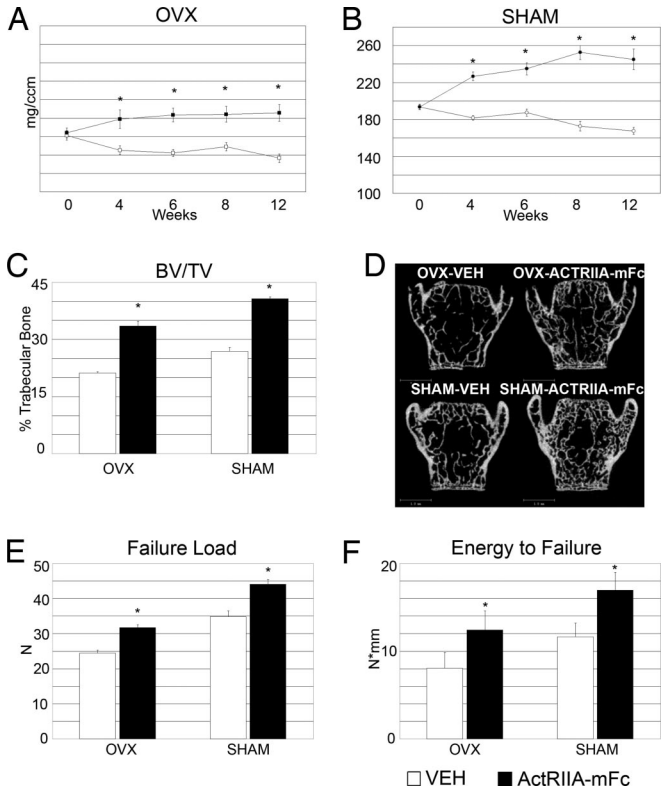

Fig. 3. ActRIIA–mFc treatment reverses trabecular bone loss in ovariectomized mice. OVX or SHAM mice were treated with ActRIIA–mFc (filled bars) or VEH (open bars) for a total of 12 weeks. *In vivo* pQCT assessment of trabecular bone density (mg/cm^3) in the proximal tibia of OVX (*A*) and SHAM (*B*) mice was determined before dosing and after 4, 6, 8, and 12 weeks of treatment. (*C*) The Tb BV/TV (%) in OVX and SHAM mice was determined by *ex vivo* μCT analysis of the fifth lumbar vertebra. (*D*) Representative images of vertebrae are shown for each treatment group. (*E*) Vertebral failure load (N) determined by compression testing from OVX- and SHAM-treated mice. (*F*) Energy-to-failure (N $\times$ mm) from OVX and SHAM. All results are reported as the mean $\pm$ SEM. *, $P < 0.01$.

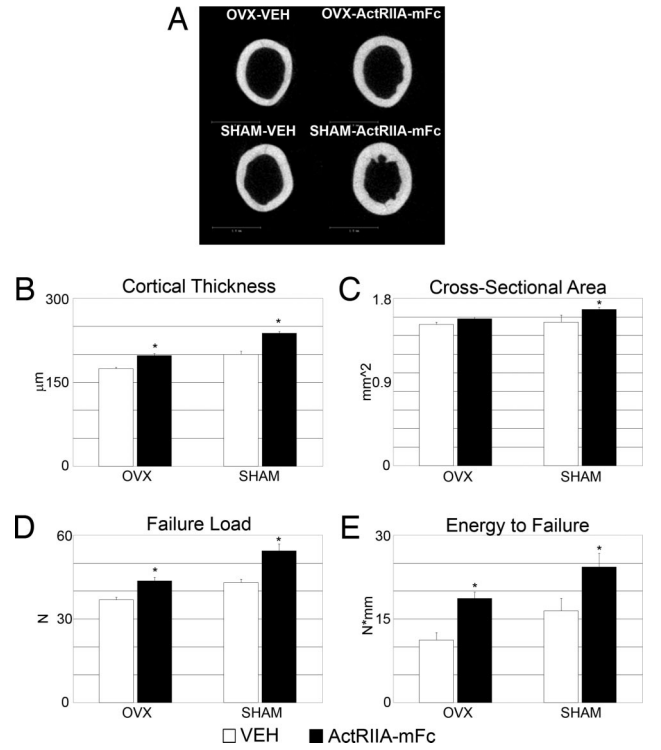

Fig. 4. ActRIIA–mFc increases cortical bone volume and improves femoral strength. Cortical bone mass and strength was assessed in the femur of VEH-treated (open bars) and ActRIIA–mFc-treated (filled bars) mice by μCT after 12 weeks of treatment. (*A*) Representative cross-sectional images of the femoral diaphysis. (*B*) The cortical thickness (μm) at the diaphysis of OVX and SHAM mice. (*C*) Total cross-sectional area (mm^2) of the femur in OVX and SHAM mice. (*D*) The failure load (N) was determined by three-point bending analysis of the femur for each group. (*E*) The energy-to-failure (N $\times$ mm) was also determined for each group. *, $P \leq 0.01$.

VEH when compared with SHAM-VEH ($P \leq 0.01$) and was higher in ActRIIA–mFc-treated OVX mice (13%) and SHAM (19%) mice relative to VEH-treated controls (Fig. 4*B*; $P \leq 0.01$ for both). The total cross-sectional area of the bone was increased in SHAM mice in response to ActRIIA–mFc treatment ($P \leq 0.01$), whereas SHAM-VEH-, OVX-VEH-, and OVX-ActRIIA–mFc-treated mice were not significantly different from each other (Fig. 4*C*). The endosteal circumference in both treatment groups were reduced when compared with the VEH-treated controls ($P \leq 0.05$) and mainly contributed to the increased cortical thickness.

To determine whether the cortical bone changes were associated with altered bone strength, three-point bending of the femur was performed. Femoral bending strength tended to be higher ($P = 0.10$), and energy-absorbed-to-failure was greater ($P \leq 0.01$) in OVX mice treated with ActRIIA–mFc relative to controls (Fig. 4 *D* and *E*). In SHAM mice treated with ActRIIA–mFc, both femoral bending strength and energy-absorbed-to-failure were higher than VEH controls (Fig. 4 *D* and *E*, $P \leq 0.01$). The OVX ActRIIA–mFc-treated mice showed similar or improved mechanical properties when compared with SHAM VEH controls, indicating rescue from the osteopenic phenotype.

Discussion

These data demonstrate that, *in vitro*, ActRIIA–mFc inhibits activin signaling through the Smad 2/3 pathway and reverses the inhibitory function of activin on human osteoblasts.

These results are consistent with a recent report demonstrating that physiologically relevant levels of activin are produced by osteoblasts and that follistatin, a direct activin antagonist (30), increases osteoblast differentiation in the presence or absence of added activin (25). Our *in vivo* data demonstrate that ActRIIA–mFc promotes dramatic increases in bone mass and strength at multiple skeletal sites because of increases in bone formation as determined by *in vivo* pQCT, dynamic histomorphometry, μCT, and biomechanical testing. The anabolic effects on bone formation induced by ActRIIA–mFc appear to be by a different mechanism than PTH. For example, histomorphometry of PTH-treated mice showed increases in osteoblast surface, osteoclast surface, and the eroded surface of bone (31), whereas those parameters showed a minor decrease at two weeks but did not show significant differences at other periods during the course of ActRIIA–mFc administration.

Our data are in contrast to previously reported results that activin may stimulate bone formation by direct administration to a fracture site or by systemic administration to aged OVX rats (26, 27). However, it is unclear whether the activin effects on fracture healing are attributable to an activin-mediated inflammatory response causing increased callus formation, which may in turn stimulate fracture healing (32). In OVX rats, systemic administration of activin at low doses increased bone mass and strength similarly to the effects of PTH. However, quantitative vertebral histomorphometry failed to demonstrate any effect of activin on any parameters including Tb BV/TV and BFR. In contrast, PTH displayed a robust stimulation of trabecular volume (27). This does not preclude the possibility that low,

intermittent dosing of activin in older animals may be able to increase bone volume.

Currently, the effects of ActRIIA–mFc treatment may not be solely due to inhibiting activin and but could be due to antagonism of other TGF-β family members. For example, BMP-3 is a proposed negative regulator of bone formation that has been reported to bind to ActRIIA, albeit at a much lower affinity of 1.8 μM K_D (33) versus activin, which binds with an affinity of 30 pM K_D (15). The effect of ActRIIA–mFc cannot be attributed exclusively to the binding of BMP-3 because treatment of Bmp-3 null mice with ActRIIA–mFc results in a 20% increase in BMD (R.S.P., unpublished observations). Additionally, ActRIIA has been reported to bind other BMP ligands including BMP-2 and BMP-7 with affinities of 36 and 3.5 μM, respectively (33). However, these ligands are able to promote bone growth, and their possible inhibition by ActRIIA–mFc would not lead to increased bone formation.

Our hypothesis that activin is a negative regulator of bone mass is supported by and clarifies reports (28, 34) exploring the role of inhibin, an activin antagonist, acting as a natural regulator of bone mass. It has been demonstrated that inducible expression of inhibin in transgenic mice led to a significant increase in bone mass and strength (28). Overexpression of inhibin resulted in increased mineral apposition rate and osteoblast number, suggestive of an anabolic effect. Additional studies by Perrin *et al.* (35) provide insight into the possible function of inhibin in postmenopausal bone loss. In perimenopause, there is a decrease in inhibin levels and a corresponding rise in FSH levels that is correlated with increased bone turnover, despite a lack of change in estrogen levels. The rise in FSH is consistent with increased activin signaling in the pituitary due to the decreased levels of inhibin. Based on the studies presented here and discussed earlier, the loss of inhibin is expected to cause increased activin signaling in bone, which may result in increased osteoclast and decreased osteoblast development, resulting in bone loss. It has been proposed that the increased FSH levels in postmenopausal women may act directly to promote osteoclastogenesis and increase bone resorption (36), although these results are considered controversial (37). Another interpretation is that increased FSH levels are merely a consequence of decreased inhibin levels and that increased activin signaling is the causal inhibin-related event leading to bone loss.

In conclusion, pharmacological blockade of ligand signaling through the ActRIIA receptor has skeletal anabolic effects and may represent a therapeutic approach to increase bone mass and strength in diseases with skeletal fragility.

Materials and Methods

Construction of ActRIIA–mIgG2a (ActRIIA–mFc) Vector. The ActRIIA extracellular domain (A34-P115) was obtained by PCR amplification. The purified PCR fragment and the pAID4 mIgG2a vector were ligated to create the expression construct, and the sequence was confirmed by double strand dideoxy sequencing.

Expression and Purification of ActRIIA–mFc. The pAID4-ActRIIA–mIgG2A construct was transiently transfected into HEK293 cells. After 1 week of growth at 37°C, the conditioned media were harvested by using a two-step column chromatography procedure. The purified ActRIIA–mFc was eluted from the column and then dialyzed into PBS.

Reporter Gene Assay. A204 cells were plated in a 48-well plate (1×10^5 cell per well) in McCoy's 5A media with 10% FBS and incubated at 37°C. The cells were transiently transfected with pGL3(CAGA)12-luc (a plasmid with the firefly luciferase gene controlled by SMAD 2/3 response element) and pRL-CMV-luc (a plasmid with *Renilla* luciferase controlled by a constitutively active CMV promoter) at a 10:1 ratio. Cells were incubated for 16 h at 37°C in fresh media with 0.1% BSA containing either activin alone (10 ng/ml) or a complex of activin and varying amount of ActRIIA–mFc preincubated for 45 min at 37°C. After 6 h, cells were lysed and assayed by using a Dual-Luciferase reporter assay kit (Promega). Results are expressed as a ratio of firefly over *Renilla* luciferase activity in relative light units.

Binding Affinity of ActRIIA–mFc. Receptor ligand-binding affinities were determined by using a Biacore 3000 instrument (GE Healthcare Life Sciences). Goat anti-murine Fc antibody (Jackson ImmunoResearch) was immobilized on two flow cells of a CM5 chip. The ActRIIA–mFc was captured on the experimental flow cell by injecting the purified protein (2 μg/ml at 10 μl/min) across the bound antibody, resulting in ≈100 resonance units of captured receptor. The receptor–antibody complex remained stable over each ligand-binding cycle. For kinetic analysis, a concentration series of activin A was injected at a flow rate of 50 μl/ml over experimental and reference antibody surfaces at 20°C. The antibody surface was regenerated between binding cycles with injection of 10 mM glycine (pH 1.7). To obtain kinetic rate constants, corrected data were fit by using BiaEvaluation software. A kinetic analysis of each receptor–ligand interaction was obtained by fitting the response data to a reversible 1:1 biomolecular interaction model. The equilibrium constant K_D was determined by the quotient K_{off}/K_{on}. Constants are reported as the average of three or more independent analyses of receptor ligand interactions.

Osteoclast Differentiation and TRAP ELISA. The mouse macrophage cell line RAW264.7 (ATTC TIB-71) was cultured in Dulbecco's modified Eagle's medium high glucose 1× (GIBCO), 10% FBS (SAFC Biosciences), 5 units of penicillin–streptomycin (Cellgro), and 0.25 μg/ml amphotericin B (Sigma-Aldrich). Osteoclast differentiation experiments were performed in 12-well plates seeded at 4×10^4 cells per well in minimal essential medium-α without phenol red (Invitrogen), 10% heat-inactivated charcoal-stripped FBS (Invitrogen) with antibiotic, and antifungal agent. Media were supplemented with 20 ng/ml RANKL (R & D Systems), 30 ng/ml MCSF (R & D Systems), ±20 ng/ml activin A (R & D Systems), and ±20 μg/ml ActRIIA–mFc. Differentiation media were changed every 2–3 days over 12 days and used for the TRAP assay (Immunodiagnostics Systems).

Osteoblast Mineralization of NHOst Cells. NHOst cells (Lonza) were cultured in minimal essential medium-α without phenol red (Invitrogen), 10% FBS (SAFC Biosciences), 5 units of penicillin–streptomycin (Cellgro), and 0.25 μg/ml amphotericin B. Mineralization experiments were performed in 12-well plates seeded at 5×10^4 cells per well. Mineralization medium was the same as above with the addition of 10% heat-inactivated charcoal-stripped FBS (Invitrogen), 20 mM Hepes (Cellgro), and 1.8 mM $CaCl_2$. Media were supplemented with 100 nM dexamethasone ,10 nM β-glycerol phosphate, ±20 ng/ml activin A (R & D Systems), and ±20 μg/ml ActRIIA–mFc. Media were changed every 2–3 days over the 14-day assay period. Cells were analyzed for bone mineral deposition by the use of the osteogenesis quantitation kit (Chemicon International). Cells were rinsed with PBS, fixed in formalin-free fixative (Sigma–Aldrich) for 15 min, and stained with alizarin red.

***In Vivo* Administration of ActRIIA–mFc.** Gonadally intact and 4-week-old OVX- or SHAM-operated C57BL/6NTac female mice were purchased from Taconic. At 12 weeks of age, mice were administered ActRIIA–mFc protein at 10 mg/kg or PBS vehicle, twice per week by i.p. injection. Mice were euthanized after 12 weeks of treatment ($n = 8$–10). Mice were injected with calcein (20 mg/kg) at 9 and 2 days before euthanasia. Mice were euthanized after 2, 4, 6, or 12 weeks of treatment. At euthanasia, the femurs, tibias, and L4/L5 vertebrae were dissected for further analysis.

All *in vivo* experiments were performed with the approval of Acceleron Pharma's Institutional Animal Care and Use Committee.

***In Vivo* pQCT.** The left tibia of anesthetized mice was analyzed during the course of the study by using an XCT Research SA+ pQCT scanner (Stratec Medizintechnik). Measurements were taken before dosing and then after 4, 6, 8, and 12 weeks of treatment with ActRIIA–mFc. CT slices at the proximal tibia were taken at 2.0 and 2.5 mm from the joint for trabecular bone and at 6.0 mm for cortical bone. Bone densities were calculated by using contour mode 1 and peel mode 2 with the provided software (version 5.50D).

***Ex Vivo* Assessment of Bone Architecture by μCT.** Femurs and vertebrae were evaluated by using a desktop microtomographic imaging system (μCT40, Scanco Medical AG) equipped with a 10-mm focal spot microfocus x-ray tube. Transverse CT slices of femoral midshaft, the distal femoral metaphysis, and vertebral body (L5) were acquired by using 12-μm isotropic voxel size as described (38). For the vertebral body, ≈220 CT slices were obtained from the cranial to caudal growth plates. Images were reconstructed, filtered, and

thresholded by using a specimen-specific threshold (39, 40). Morphometric parameters were computed by using a direct three-dimensional approach that does not rely on any assumptions about the underlying structure. For trabecular morphology, volume fraction (BV/TV, %), trabecular thickness (TbTh, μm), trabecular separation (TbSp, μm), and TbN (mm^{-1}) were assessed. For midfemoral cortical bone, the total cross-sectional area (TA, mm^2), cortical bone area (mm^2), bone area fraction (%), and cortical thickness (μm) were assessed.

Biomechanical Testing. Studies of the biomechanical properties of the femur in three-point bending and of the vertebral body in compression assays were performed as described (37–39). Load was applied at a constant rate (0.05 mm/s) until failure. The failure load (*N*), bending stiffness (*N*/mm), and work-to-failure ($N \times$ mm) were measured from the load-displacement curve.

Bone Histomorphometric Analysis. Static and dynamic histomorphometry was performed after 2, 4, 6, and 12 weeks of treatment. Femurs were processed as described (41) and stained with 0.1% toluidine blue (pH 6.4), or Von Kossa. Static parameters of bone formation and resorption were measured in a defined area between 725 and 1,270 μm from the growth plate by using an OsteoMeasure bone histomorphometry system (Osteometrics). For static parameters, the Tb BV/TV, TbN (mm), TbTh (μm), NOb/BPm (mm^{-1}) and NOc/Bpm (mm^{-1}) per bone perimeter, and ES/BS (%) were measured. For dynamic histomorphometry, MS/BS (%) and mineral apposition rate (μm/day) were measured in unstained sections under UV light and used to calculate BFR ($\mu m^3/\mu m^2$/day), as described (41). The terminology and units used are those recommended by the Histomorphometry Nomenclature Committee of the American Society for Bone and Mineral Research (42).

For additional details on on materials and methods used, see *SI Materials and Methods*.

1. Rodan GA (1997) Bone mass homeostasis and bisphosphonate action. *Bone* 20:1–4.
2. Lambrinoudaki I, Christodoulakos G, Botsis D (2006) Bisphosphonates. *Ann NY Acad Sci* 1092:397–402.
3. Black DM, *et al.* (2003) The effects of parathyroid hormone and alendronate alone or in combination in postmenopausal osteoporosis. *N Engl J Med* 349:1207–1215.
4. MacDonald BR, Gowen M (2001) Emerging therapies in osteoporosis. *Best Pract Res Clin Rheumatol* 15:483–496.
5. Burr D (2003) Microdamage and bone strength. *Osteoporosis Int* 14 (Suppl 5):67–72.
6. Robling AG, Castillo AB, Turner CH (2006) Biomechanical and molecular regulation of bone remodeling. *Annu Rev Biomed Eng* 8:455–498.
7. Garrett IR (2007) Anabolic agents and the bone morphogenetic protein pathway. *Curr Top Dev Biol* 78:127–171.
8. Canalis E, Giustina A, Bilezikian JP (2007) Mechanisms of anabolic therapies for osteoporosis. *N Engl J Med* 357:905–916.
9. Neer RM, *et al.* (2001) Effect of parathyroid hormone (1–34) on fractures and bone mineral density in postmenopausal women with osteoporosis. *N Engl J Med* 344:1434–1441.
10. Liu H, *et al.* (2006) The cost-effectiveness of therapy with teriparatide and alendronate in women with severe osteoporosis. *Arch Intern Med (Moscow)* 166:1209–1217.
11. Gazzerro E, Canalis E (2006) Bone morphogenetic proteins and their antagonists. *Rev Endocr Metab Disorders* 7:51–65.
12. Swiontkowski MF, *et al.* (2006) Recombinant human bone morphogenetic protein-2 in open tibial fractures. A subgroup analysis of data combined from two prospective randomized studies. *J Bone Jt Surg Am* 88:1258–1265.
13. Garrison KR, *et al.* (2007) Clinical effectiveness and cost-effectiveness of bone morphogenetic proteins in the non-healing of fractures and spinal fusion: A systematic review. *Health Technol Assess* 11:1-iv.
14. Vale W, *et al.* (1986) Purification and characterization of an FSH releasing protein from porcine ovarian follicular fluid. *Nature* 321:776–779.
15. del Re E, *et al.* (2004) Reconstitution and analysis of soluble inhibin and activin receptor complexes in a cell-free system. *J Biol Chem* 279:53126–53135.
16. Donaldson CJ, *et al.* (1999) Activin and inhibin binding to the soluble extracellular domain of activin receptor II. *Endocrinology* 140:1760–1766.
17. Vale W, Bilezikian JP, Rivier C (1994) Reproductive and other roles of inhibins and activins. *The Physiology of Reproduction*, eds Knobil E, Neill JD (Raven, New York), pp 1861–1878.
18. Lewis KA, *et al.* (2000) Betaglycan binds inhibin and can mediate functional antagonism of activin signaling. *Nature* 404:411–414.
19. Martens JW, *et al.* (1997) Inhibin interferes with activin signaling at the level of the activin receptor complex in Chinese hamster ovary cells. *Endocrinology* 138:2928–2936.
20. Rivier C, Rivier J, Vale W (1986) Inhibin-mediated feedback control of follicle-stimulating hormone secretion in the female rat. *Science* 234:205–208.
21. Wiater E, Vale W (2003) Inhibin is an antagonist of bone morphogenetic protein signaling. *J Biol Chem* 278:7934–7941.
22. Ogawa Y, *et al.* (1992) Bovine bone activin enhances bone morphogenetic protein-induced ectopic bone formation. *J Biol Chem* 267:14233–14237.
23. Fuller K, Bayley KE, Chambers TJ (2000) Activin A is an essential cofactor for osteoclast induction. *Biochem Biophys Res Commun* 268:2–7.
24. Sakai R, *et al.* (1993) Activin enhances osteoclast-like cell formation *in vitro*. *Biochem Biophys Res Commun* 195:39–46.
25. Eijken M, *et al.* (2007) The activin A-follistatin system: Potent regulator of human extracellular matrix mineralization. *FASEB J* 21:2949–2960
26. Sakai R, Miwa K, Eto Y (1999) Local administration of activin promotes fracture healing in the rat fibula fracture model. *Bone* 25:191–196.
27. Sakai R, *et al.* (2000) Activin increases bone mass and mechanical strength of lumbar vertebrae in aged ovariectomized rats. *Bone* 27:91–96.
28. Perrien DS, *et al.* (2007) Inhibin A is an endocrine stimulator of bone mass and strength. *Endocrinology* 148:1654–1665.
29. Dennler S, *et al.* (1998) Direct binding of Smad3 and Smad4 to critical TGF beta-inducible elements in the promoter of human plasminogen activator inhibitor-type 1 gene. *EMBO J* 17:3091–3100.
30. Nakamura T, *et al.* (1990) Activin-binding protein from rat ovary is follistatin. *Science* 247:836–838.
31. Yamaguchi M, *et al.* (2005) Insulin receptor substrate-1 is required for bone anabolic function of parathyroid hormone in mice. *Endocrinology* 146:2620–2628.
32. Jones KL, *et al.* (2007) Activin A is a critical component of the inflammatory response, and its binding protein, follistatin, reduces mortality in endotoxemia. *Proc Natl Acad Sci USA* 104:16239–16244.
33. Allendorph GP, *et al.* (2007) BMP-3 and BMP-6 structures illuminate the nature of binding specificity with receptors. *Biochemistry* 46:12238–12247.
34. Gaddy-Kurten D, *et al.* (2002) Inhibin suppresses and activin stimulates osteoblastogenesis and osteoclastogenesis in murine bone marrow cultures. *Endocrinology* 143:74–83.
35. Perrien DS, *et al.* (2006) Bone turnover across the menopause transition: Correlations with inhibins and follicle-stimulating hormone. *J Clin Endocrinol Metab* 91:1848–1854.
36. Sun L, *et al.* (2006) FSH directly regulates bone mass. *Cell* 125:247–260.
37. Baron R (2006) FSH versus estrogen: Who's guilty of breaking bones? *Cell Metab* 3:302–305.
38. Glatt V, Canalis E, Stadmeyer L, Bouxsein ML (2007) Age-related changes in trabecular architecture differ in female and male C57BL/6J mice. *J Bone Miner Res* 22:1197–1207.
39. Leung CK, Lam FK (1996) Performance analyses for a class of iterative image thresholding algorithms. *Pattern Recognit* 29:1523–1530.
40. Ridler TW, Calvard S (1978) Picture thresholding using an iterative selection method. *IEEE Trans Syst Man Cybern* 8:630–632.
41. Gazzerro E, *et al.* (2005) Skeletal overexpression of gremlin impairs bone formation and causes osteopenia. *Endocrinology* 146:655–665.
42. Parfitt AM, *et al.* (1987) Bone histomorphometry: Standardization of nomenclature, symbols, and units. Report of the ASBMR Histomorphometry Nomenclature Committee. *J Bone Miner Res* 2:595–610.